

GP-net: Grasp Proposal for Mobile Manipulators

Anna Konrad
Hamilton Institute
Maynooth University
anna.konrad.2020@mumail.ie

John McDonald
Department of Computer Science
Maynooth University
john.mcdonald@mu.ie

Rudi Villing
Department of Electronic Engineering
Maynooth University
rudi.villing@mu.ie

Abstract—We present the Grasp Proposal Network (GP-net), a Convolutional Neural Network model which can generate 6-DOF grasps for mobile manipulators. To train GP-net, we synthetically generate a dataset containing depth-images and ground-truth grasp information for more than 1400 objects. In real-world experiments we use the EGAD! grasping benchmark to evaluate GP-net against two commonly used algorithms, the Volumetric Grasping Network (VGN) and the Grasp Pose Detection package (GPD), on a PAL TIAGo mobile manipulator. GP-net achieves grasp success rates of 82.2% compared to 57.8% for VGN and 63.3% with GPD. In contrast to the state-of-the-art methods in robotic grasping, GP-net can be used out-of-the-box for grasping objects with mobile manipulators without limiting the workspace, requiring table segmentation or needing a high-end GPU. To encourage the usage of GP-net, we provide a ROS package along with our code and pre-trained models at <https://aucoroboticsmu.github.io/GP-net/>.

Index Terms—grasping, robotics, neural networks, mobile manipulator, 6-DOF grasps, ROS

I. INTRODUCTION

Manipulation is an ongoing and challenging problem in robotics due to its complexity and variability. Grasping objects is largely solved in industrial settings with known objects and fixed, foreknown poses of the object and robot. However more complex, dynamic and unstructured environments are still an active field of research. Before the era of machine learning, analytical approaches were widely tested in simulation, but had limited applicability in real-world scenarios due to noisy or partial data [1]. With the rise of computational power, researchers have switched to data-driven approaches which are more robust to real world conditions. To simplify the problem, these solutions initially focused on fixed, overhead cameras and a reduced grasp space with 4 Degrees-of-Freedom (DOF) grasps [2]–[7], i.e. top-grasps which can vary their pose in 3D position and one rotational axis.

However, when moving those scenarios outside of a lab environment, the restriction to top-grasps limits the applicability of the algorithms, while 6-DOF grasps can enhance reachability for the robots. Furthermore, methods have to cope with pose changes of the camera and be robust to noise, different lighting conditions and much more. There are efforts being made towards solutions for all of these problems, for example with 6-DOF grasp proposal algorithms [8]–[12],

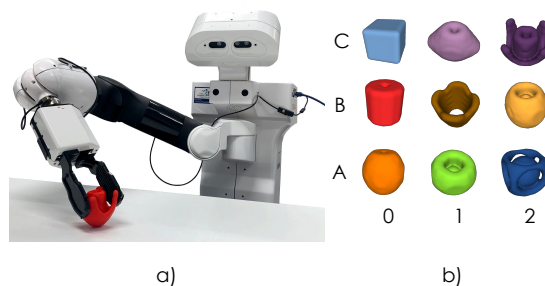


Fig. 1. a) Our PAL TIAGo robot grasping an object. b) The 9 test objects from the EGAD! benchmark used for the real-world experiments.

closed-loop grasping [5], [13], [14], or grasping transparent objects [15].

Applying these algorithms to mobile robots (robots that have a mobile base) often proves difficult. The ability of mobile robots to move within their environment increases the range of possible use-cases, but also increases the range of potential poses of the object with respect to the robot. While there exist algorithms that can be used on mobile robots to propose grasps, they typically need table segmentation to filter the grasp proposals [11] or 3D object detection to define the workspace [8]. Other solutions require wrist-mounted depth cameras [14] or high-end GPUs for running inference [9]. We identify a need for a flexible method that can be used on mobile robotic devices without requiring 3D object detection for defining the workspace, table segmentation for filtering grasp proposals, or high-end GPUs for performing inference.

We therefore present GP-net, a grasp proposal network that can predict 6-DOF grasps. It can be used to grasp single, unknown objects from planar surfaces like tables or furniture units with mobile manipulators. In real-world experiments using 9 objects of the EGAD! grasping benchmark [16] with a PAL TIAGo manipulator (see Figure 1), GP-net achieves a grasp success rate of 82.2%, outperforming the Volumetric Grasping Network (VGN) with 57.8% and the Grasp Pose Detection package (GPD) with 63.3%.

In contrast to VGN and GPD, GP-net works without the need to perform additional pre-processing steps or 3D object detection and therefore can be applied directly to the camera input. GP-net can be used out-of-the-box to propose grasps based on depth images from a mobile manipulator with a head-mounted camera. The contributions of this work can be

summarised as follows:

- GP-net: a model to predict 6-DOF grasps out-of-the-box for a PAL TIAGo mobile manipulator employing a parallel jaw gripper without the need to specify the workspace or run table segmentation to filter grasp poses.
- A ROS package to run GP-net to produce grasp proposals from a depth camera.
- A dataset to train GP-net or alternative network architectures. Furthermore, we make our code available so it can be used to train GP-net to adapt to different robots or grippers.

II. BACKGROUND AND RELATED WORK

Grasping objects involves a lot of variation and uncertainty in the real world with unknown object shapes, unknown poses of the robot and objects, and noisy sensor readings. To solve this high dimensional problem, early analytical approaches constrained and simplified the problem by making assumptions about the contacts, friction, and the geometric and physical model of the objects. Consequently, these approaches were usually only tested in simulation with accurate knowledge about the object, robot and environment and without the need to contend with noisy sensor measurements [1].

With the surge of data-driven approaches, analytical methods have been supplanted by machine learning algorithms for sampling grasp poses [1]. Initially, these methods often used 4-DOF top-grasps, where the gripper approaches the object top-down and can only rotate around the approach axis. Furthermore, the initial methods were usually discriminative [17], where grasp configurations are sampled and subsequently ranked according to a quality metric [2], [3], [18], [19]. While discriminative methods showed good grasping performance, algorithms directly proposing good grasp configurations in a generative manner can improve inference time significantly and enable grasping in real-time [4]–[8].

To make robotic grasping usable in less constrained environments, the algorithms must be able to propose 6-DOF grasp poses while coping with varying camera viewpoints and object poses. These requirements increase the search-space for possible grasps and therefore the difficulty of the problem significantly. While modern algorithms are able to find robust grasp poses in this increased search space, they often suffer from problems such as high latency [20], high computational requirements [9], or limitations to the robot workspace [8].

Generally, comparing performance of different methods proves difficult due to different robots, grippers and objects being used. Usually, algorithms are tested on household objects without the opportunity to reproduce the experiments or compare performance [2], [8]–[11], [20]–[22]. More recently, promising benchmarks like EGAD! [16] using 3D-printed objects have been proposed to generalise the testing of grasping algorithms and improve the comparability and reproducibility of experiments. For this reason, we use EGAD! objects in our real-world experiments, see Section V-A.

One of the first methods that could be directly applied to find 6-DOF grasp poses based on point-clouds is the Grasp Pose

Detection (GPD) package [11]. It identifies a region of interest, samples grasp proposals, encodes the grasp proposals in a multi-channel image and finally uses a Convolutional Neural Network to predict the grasp quality. While it is widely used due to its availability in a ROS package, we find that it mostly suggests grasps on the table plane if run without a prior table-segmentation. Further, the discriminative sampling nature of the algorithm leads to high latencies, taking an average of $15.2s$ to propose grasps in our experiments, see Section V-A.

A family of approaches that was mostly proposed after GPD reconstructs the grasping surface into meshes [10], [20], point clouds [22] or signed distance functions [8], [21] and uses the new representation to predict 6-DOF grasps. One of these approaches, the Volumetric Grasping Network (VGN) [8], exhibits promising results by predicting grasp proposals from a truncated signed distance function (TSDF). Once the TSDF is built, grasp proposals can be predicted in real-time within $10ms$, opening up possibilities for closed-loop control.

VGN achieves a grasp success rate of 80% in real-world experiments using household objects. However, the acquisition of the TSDF is achieved by integrating a stream of depth images acquired by a wrist-mounted depth camera, where the camera follows a pre-defined scan trajectory around a defined workspace. When applying VGN to mobile robots, the position of the object would have to be estimated in advance to set the x-y coordinates and the height of the workspace around the object. Furthermore, if no wrist-mounted camera is available, the TSDF must be built from the incoming depth images of the head-mounted camera, which affects the quality of the TSDF. Overall, this limits the applicability of VGN on mobile manipulators.

Another recent and promising method, Contact-GraspNet [9], proposes 6-DOF grasps from a single pointcloud. The method achieves a grasp success rate of more than 90% in real-world experiments using a set of household objects. However, the model implementation requires a GPU with $\geq 64GB$ RAM for training and $\geq 8GB$ RAM for inference. Such requirements make Contact-GraspNet unsuitable for usage on mobile robotic platforms that do not have access to high-end dedicated GPUs, as is the case for several currently available mobile manipulators [23], [24].

From the literature it is clear that there are few methods that can be used out-of-the-box to identify 6-DOF grasps for unknown objects in unknown poses with mobile manipulators. In particular, there are no methods available that can be run on mobile manipulators without the need to run pre-processing such as plane segmentation to filter grasp proposals or 3D object detection to identify the workspace. We propose GP-net to fill this gap and provide a ROS package that can be used to generate 6-DOF grasp proposals on mobile manipulators without any additional pre-processing.

III. GRASP PROPOSAL NETWORK

We consider the problem of proposing 6-DOF grasps for a mobile manipulator with a parallel-jaw gripper and a head-mounted RGB-D camera. The environment consists of a single

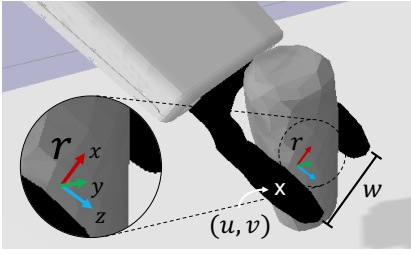


Fig. 2. Visualisation of the contact-based grasp representation with visible grasp contact coordinates in the image (u, v) , grasp orientation r and grasp width w .

object $o \in \mathcal{O}$ placed on a planar surface. The object is placed in a stable resting pose with the robot in grasping-range. The goal is to propose a diverse set of 6-DOF grasps $g \in \mathcal{G}$ for the object based on a depth image \mathcal{I} .

Similar to Sundermeyer et al. [9], we represent grasps based on the contact point between the gripper and the object. Each pixel (u, v) in a depth image \mathcal{I} describes a potential grasp contact, i.e. the contact of a gripper plate during grasp execution. The full grasp is defined as $g \in (u, v, q, r, w)$, with the grasp quality q , the orientation of the grasp in camera coordinates r and the width of a grasp w . A visualisation of the grasp representation is depicted in Figure 2.

We base the network architecture for GP-net on a ResNet-50 model pre-trained on ImageNet. A description of the pipeline and the output tensor of the model can be seen in Figure 3. Since the rendered depth images consist of one channel and the pre-trained ResNet-50 architecture uses 3 input channels, we apply a jet-colourscale to the depth image as described by Eiter et al. [25]. We set fixed normalisation boundaries of $0.4m$ and $1.4m$ to keep the relation to the real distance of a given scene. Note that points closer than $0.4m$ cannot be seen by our depth camera and points further away than $1.4m$ are out of the grasping range of the robot.

GP-net outputs six channels with the same size as the input image. Each pixel in the output tensor represents a grasp whose visible contact point corresponds to that pixel, with the channels defining the quality of the grasp q , the grasp orientation r in form of a quaternion, and the width of the grasp w . Similar to VGN [8], we normalise the quaternions to unit quaternions and apply a sigmoid function to the quality channel.

Loss function: Since creating ground-truth grasp proposals for training at each pixel is computationally infeasible, we generate sparse maps containing grasp information at visible grasp contacts for up to 100 pre-sampled grasps per object. The process of generating the training data is described in Section IV. We backpropagate the loss only through the output pixels at which we have ground-truth grasp information, similar to VGN [8]. We define our loss function as:

$$\mathcal{L} = \mathcal{L}_q + q(\alpha\mathcal{L}_r + \beta\mathcal{L}_w) \quad (1)$$

with \mathcal{L}_q being the binary cross-entropy loss between the ground-truth and predicted binary quality values, q and \hat{q} ,

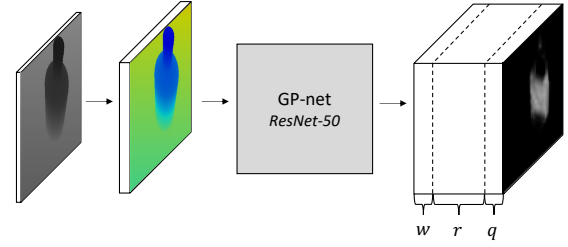


Fig. 3. Using a depth image as input, we apply a jet-colourscale, process the image with GP-net and output pixel-wise grasp proposals with a quality q , orientation r and grasp width w .

$\mathcal{L}_r = 1 - |r \cdot \hat{r}|$ the distance between the target and predicted quaternions [26], r and \hat{r} , and \mathcal{L}_w the L1 loss between the ground-truth and predicted grasp width, w and \hat{w} . Since negative grasps do not have valid configurations for the model to learn, we use the ground-truth binary quality of the grasps, q , to control whether the second part of the loss function is included. We set $\alpha, \beta = 0.1$, which we experimentally found to give a good balance between \mathcal{L}_q , \mathcal{L}_r and \mathcal{L}_w .

In contrast to the loss function of VGN [8], we only allow one valid configuration for the orientation loss \mathcal{L}_r . This change is rooted in the grasp contact representation which removes the symmetry of the two orientation configurations by anchoring the grasps on the visible grasp contact. Since the x-axis of the grasp coordinate frame points towards the second grasp contact (see Figure 2), there remains only one valid orientation. This representation does not affect grasp variability since the parallel-jaw gripper is symmetric.

Using the model output for robotic grasping: To use the output of GP-net for grasping objects with a robot, it has to be transformed into grasp proposals. As a first step, a maximum of $j = 5$ grasps are chosen from the output tensor using non-maximum suppression with a peak-distance of 4 pixels and an acceptance threshold of $\gamma = 0.1$. Note that the acceptance threshold γ for applying non-maximum suppression defines the minimum predicted quality \hat{q} that will result in a grasp proposal. Once the image coordinates (u, v) for those grasp contacts are chosen, we re-project them into 3D camera coordinates using the camera intrinsics K and the depth value of (u, v) in the input depth image. Using the predicted quaternion \hat{r} and the predicted width \hat{w} of each grasp, we translate the grasp contact to the tool centre point by moving them $0.5\hat{w}$ along the grasp x-axis between the gripper plates. As a last step, the grasp is transformed from the camera coordinate frame to the robot base coordinate frame.

Our ROS package provides this functionality by running inference with a trained model, selecting the best grasps and mapping them to the robot base transform. Further, we provide example code to use the package with a pre-trained GP-net model to plan grasps for a PAL TIAGo robot using a parallel jaw gripper. If using other gripper configurations, our code can be used to generate an adjusted dataset, train a new model and use the new model with our ROS package to produce appropriate grasp proposals.

IV. TRAINING DATASET

To train GP-net, we render a synthetic depth-image based dataset with sparse ground-truth grasp information. Similar to DexNet2.0 [2], we use the objects from the 3Dnet [27] and KIT [28] mesh datasets. When loading the 3D meshes from the mesh datasets, we re-scale them to fit into TIAGo’s gripper, a parallel gripper manufactured by PAL robotics with an opening width of 8cm [29]. Re-scaling 3D meshes is commonly used to generate robotic grasping datasets. In contrast to the re-scaling methods in [2], [16], [30], we re-scale objects to a randomly chosen width drawn uniformly from the range 6cm to 10cm . In this way, our dataset includes objects which do not fit in our robotic gripper, which is a situation that will occur in real-world environments.

After re-scaling each object o , we calculate up to 25 stable resting poses $\mathcal{S}(o)$ and use the antipodal grasp sampler proposed in [2] to generate up to 100 parallel-jaw grasps $\mathcal{G}(o)$. Grasps are sampled by randomly choosing a surface point from the mesh and then sampling the grasp x-axis (see Figure 2) based on the friction cone of the surface point. This procedure does not necessarily yield the best grasp for a grasp contact point. As our dataset should contain good grasps for a contact if they are available, we modify this procedure to generate $k = 6$ potential grasps for a given contact. We calculate the computationally inexpensive robust force closure metric ϵ [31]–[33] for each of the sampled grasps at one contact point and keep the one with the highest ϵ . Using this method, we generate a total of 148,706 ground-truth grasps for the object meshes in our dataset.

Since the robust force closure metric ϵ of a sampled ground-truth grasp depends on the grasp contacts, it is consistent for any grasp approach axis, i.e. the direction of the z-axis in Figure 2. However, collisions between the gripper, object and planar surface further influence the success of a grasp. We define the quality q of a grasp in our rendered dataset as

$$q(g) = \begin{cases} 1 & \epsilon \geq \delta \text{ and } \text{coll_free}(g) \\ 0 & \text{otherwise} \end{cases} \quad (2)$$

with $\delta = 0.5$ being the robustness threshold and $\text{coll_free}(g)$ indicating if a grasp is collision free, similar to DexNet2.0 [2].

We aim to choose reproducible grasp orientations for a given scene and ground-truth grasp. In order to achieve this, we apply the following steps for choosing the grasp approach axis orientation for a given grasp: To check for collisions, we hinge-rotate the grasps in steps of $\Delta\omega = 15\text{deg}$ around the contact points and thereby the grasp x-axis (see Figure 2). If we have collision-free grasps within those orientations, we set the ground-truth grasp orientation as the median collision-free grasp. If we have multiple collision-free regions, we choose the median collision-free grasp whose approach is more aligned with the principal ray of the camera, e.g. approaching from the front of the object rather than from behind the object. With these steps, we fully define each grasp orientation in our dataset in a reproducible way.

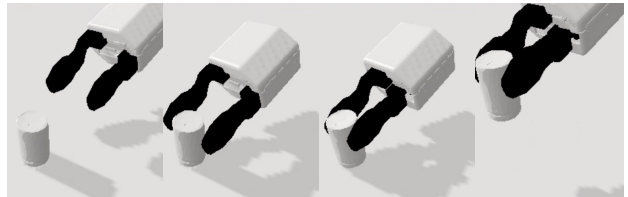


Fig. 4. One simulation trial in our analysis. A randomly chosen object is placed on a planar surface and grasped by a PAL parallel jaw gripper based on grasp proposals from GP-net.

We render $n = 20$ images for each stable pose $s \in \mathcal{S}(o)$ of each object $o \in \mathcal{O}$ from camera poses selected uniformly at random as described in VGQ-CNN [34]. We then project the grasp contacts into the image plane and calculate the image coordinates of the visible contact (u, v) . If there are multiple collision-free grasp contacts visible at one pixel, we choose the grasp with the highest robust force closure value ϵ . In addition, we store the binary segmask of the object and use the pixels not showing the object as ground-truth negative grasp contacts during training. The full dataset consists of 260,340 images with an average of 88.1 grasps per image.

V. EXPERIMENTS

We train GP-net for 20 epochs using an Adam optimiser with a learning rate of $3e^{-4}$ and a batch size of 32. Using two NVIDIA GeForce RTX 3090 GPUs, the training takes approximately 1.5 days to complete. To reduce the sim-to-real-gap for GP-net, we simulate depth-camera noise on our depth images using the noise model described in [35], [36]. We find that compared to the Gaussian noise model suggested in DexNet2.0 [2], the added depth-camera noise model significantly improves the robustness of GP-net in real-world scenarios.

A. Results

We evaluate the performance of GP-net with simulation and real-world experiments. The simulation analysis is used to validate our model and conduct the ablation studies in Section V-B since it requires less time and fewer resources than tests with a real robot. For the real-world experiments, we use GP-net on a PAL TIAGo mobile manipulator to grasp a number of objects taken from the EGAD! grasping benchmark [16]. We repeat the real-world experiments with VGN [8] and GPD [37] and compare them to the performance of GP-net.

Simulation experiments: We test the grasp success of the grasps proposed by GP-net in simulation using the pybullet [38] physics engine based on the simulation environment developed for VGN [8]. A parallel jaw gripper is simulated to approach the grasp pose linearly along the grasp z-axis for 0.15m , close the gripper using a maximum force of 5N and lift the object. The grasp is labeled as successful if the gripper is able to lift the object 0.1m above the planar surface. A visualisation of the process is depicted in Figure 4. For each trial, one of 130 objects is chosen randomly and

placed in a random position within the workspace within a $30 \times 30\text{cm}$ workspace on a planar surface. Then, a depth-image is rendered from a camera pose sampled uniformly at random from the spherical coordinates around the centre of the workspace. We run inference with GP-net on the depth image and map the resulting grasp maps to grasp proposals as described in Section III.

We simulate all grasps proposed by the model for one trial and reset the simulation environment to its initial state after each grasp attempt. Each experimental run comprises 100 such trials. We repeat each experimental run 10 times to check consistency of the model. In simulation, GP-net achieves a mean grasp success of 75.1% with a standard deviation of 2.9%.

Real-world experiments: We test the grasp success in real-world experiments with a PAL TIAGo mobile manipulator [23]. For reproducibility, we use 9 objects from the EGAD! grasping benchmark [16] (see Figure 1a) for the experiments. The objects are rescaled to fit the width of TIAGo’s gripper. Since physical experiments with all 49 test objects of the benchmark would be too time consuming, we focus on the first three stages of shape complexity and grasp difficulty. Following this method, we use the objects A-C and 0-2 of the EGAD! test objects. For each object, a total of 10 grasp trials are executed. We use two different initial robot poses for grasp-planning, each having a different head tilt and torso height, and test 5 trials in each pose of the robot. The object is placed within a $30 \times 30\text{cm}^2$ square on the table by a human operator before each grasp trial.

To compare our method with existing approaches for 6-DOF grasping, we perform the same experiments with VGN [8] and GPD [37]. To apply VGN to our scenario, we need to define the $30 \times 30 \times 30\text{cm}^3$ workspace in which the algorithm searches for grasps. We identify the table plane by applying a least squares fit to all points in the point cloud 0.2m above and not more than 1.4m in front of the base of the robot. We further limit the x and y position of the workspace to be centred and 60cm in front of the robot. Setting the workspace for VGN in more realistic scenarios with mobile manipulators would require some form of 3D object detection or an increased size of the workspace. Furthermore, VGN was originally intended to be used with a wrist-mounted depth camera performing a grasp-scan trajectory to build the TSDF. Since the focus of our work is proposing grasps from a single depth image, we instead apply VGN by building the TSDF from a single image to make it comparable to our approach.

To prevent GPD from sampling grasps on the table plane, we index the point cloud with points where grasps should be sampled. We do this by fitting a plane to the table in the same way as for VGN and subsequently calculate the distance from each point in the point cloud to the plane. If the distance of a point to the fitted plane is $\geq 0.03\text{m}$, we index the point as a potential grasp sampling point for GPD. While these approaches work for our experimental setting, the table segmentation can easily fail in other cases. GP-net does not need any workspace definition and can therefore be directly

TABLE I
REAL-WORLD EXPERIMENTS WITH A PAL TIAGO ROBOT EXECUTING 90 GRASP ATTEMPTS ON 9 OBJECTS FROM THE EGAD! BENCHMARK

	Grasp success	Grasp proposal [s]	Path planning [s]	Grasp execution [s]
GP-net (ours)	82.2%	2.5	4.4	13.8
VGN [8]	57.8%	5.0	2.8	14.4
GPD [37]	63.3%	15.2	7.2	13.5

TABLE II
NUMBER OF SUCCESSFUL GRASPS PER OBJECT FROM THE EGAD! BENCHMARK WITH A PAL TIAGO ROBOT

	A0	A1	A2	B0	B1	B2	C0	C1	C2
GP-net (ours)	10	10	6	9	10	9	6	10	4
VGN [8]	5	8	5	7	5	4	3	8	7
GPD [37]	9	7	4	8	8	6	5	5	5

applied to the depth image.

We run the algorithms for all methods on an Intel i7-10750H CPU and NVIDIA RTX 2060 GPU. The average grasp success and planning times are reported in Table I. GP-net performs better than GPD and VGN with a grasp success rate of 82.2% compared to their 63.3% and 57.8%, respectively. Comparing the number of successful grasps per object in Table II, we notice that GP-net seems to have a significant advantage when grasping round objects, often leading to successful grasps in 10/10 attempts. Note that while the grasp success rate for VGN with 57.8% is significantly lower than the 80% reported by the authors [8], they used a pre-defined scan trajectory to build the TSDF rather than a single image as here.

B. Ablation studies

To further investigate the performance of GP-net, we conduct a set of ablation studies. We investigate how an alternative grasp representation defining the Tool Centre Point (TCP) performs compared to the contact-based grasp representation (see Figure 2) used for GP-net. Further, we run simulation experiments and investigate how different acceptance thresholds γ for the non-maximum suppression influence the grasp success rate and the final number of grasp proposals.

Grasp representation: The grasp representation used in GP-net is contact-based, with each pixel representing a visible grasp contact of a potential grasp, see Section III. This grasp representation was first proposed in Contact-Graspnet [9], suggesting it facilitates the learning process by reducing the dimensionality. However, the grasp representation was not compared to conventional, TCP-based grasp representations as used in most of the related work [2]–[8], [10]–[12].

While the contact-based grasp representation can potentially increase the network performance, using this grasp representation can lead to problems in situations where no grasp contact is visible. For example if a robot is supposed to grasp a book, but is facing the spine of the book head-on. In this situation the areas for potential grasp contacts on the left and right side

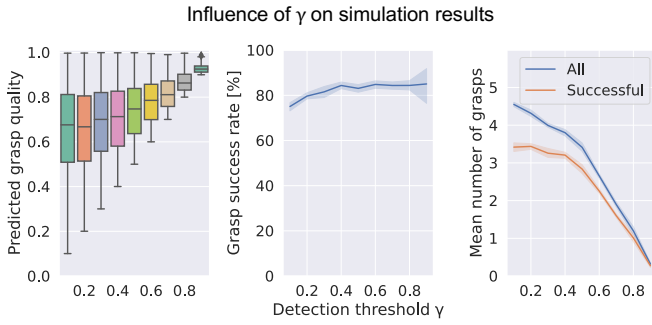


Fig. 5. Simulation results showing the influence of varying the acceptance threshold γ on the predicted quality of grasp proposals, the grasp success rate and the mean number of grasps with a 95% confidence interval.

are not visible and a contact-based method would not be able to produce valid grasp configurations. Here, a repositioning of the robot would be necessary.

For this reason we compare the performance of a contact-based grasp representation to a TCP-based grasp representation. We modified GP-net to use a TCP-based grasp representation as $g \in (u, v, z, q, r, w)$ with (u, v) being the image coordinates of the grasp centre and z being the distance between the grasp centre and the visible surface depth at (u, v) . We train the model on our dataset as described in Section V-A and compare performance to GP-net using the simulation analysis. Due to the extra variable z in the grasp representation, the model has seven output channels and we define the loss function as:

$$\mathcal{L} = \mathcal{L}_q + q(\alpha\mathcal{L}_r + \beta\mathcal{L}_w + \nu\mathcal{L}_z) \quad (3)$$

with \mathcal{L}_z being the L1 loss between ground-truth z and predicted grasp distance \hat{z} . We set $\alpha, \nu = 0.1$ and $\beta = 0.01$, since the width is not needed to predict the grasp position for the TCP-based grasp representation. After training the model for 20 epochs, we achieve a grasp success of $40.0\% \pm 4.4\%$ in simulation, significantly lower than GP-net’s $75.1\% \pm 2.9\%$ with the contact-based grasp representation. We find that the rotation loss \mathcal{L}_r plateaus at almost double that of GP-net’s loss with 0.24 for the TCP-based grasp representation and 0.13 with the contact-based grasp representation.

We hypothesise that this difference is rooted in the reduction of ambiguities when grasps are anchored to their grasp contact points. Ground-truth positive grasps would have similar orientations for neighbouring grasp contacts on an object, while TCP-based grasps could approach the same TCP position from a variety of angles. This is especially apparent when looking at cylindrical objects, where a TCP-based ground truth positive grasp could rotate the grasp axis to any orientation around the centre of the cylinder, while a contact-based ground truth positive grasp only permits one orientation such that the x-axis of the grasp passes through the centre of the cylinder (see Figure 2).

Acceptance threshold γ : The acceptance threshold γ defines the minimum predicted grasp quality \hat{q} of acceptable

grasps in the output of GP-net. Non-maximum suppression applied to these acceptable grasps yields the final grasp proposals. As such, this parameter balances the number of grasps that are proposed for a given object and the confidence the model has in the performance of those grasps. Ideally, γ should be set to propose as many grasps as possible on all type of objects while retaining a good confidence on the quality of those grasps. To investigate how this trade-off affects GP-net, we apply a range of acceptance thresholds $\gamma = [0.1, 0.2, \dots, 0.9]$ to GP-net and investigate the influence on grasp performance in simulation.

The results can be seen in Figure 5. While γ influences the minimum predicted grasp quality used for a grasp proposal, we observe the median grasp quality stabilises around 0.7 at $\gamma \leq 0.4$. This is due to γ being used only as cut-off point when applying non-maximum suppression, ensuring that grasps with higher predicted grasp qualities are proposed when available. Furthermore, even though we introduce more unsuccessful grasps for $\gamma < 0.4$ with the grasp success rate starting to drop, the average number of successful grasps still increases up to 3.4 grasps at $\gamma = 0.1$. Since no grasp proposals for an object means we are unable to grasp the object, we prioritise the average number of successful grasps over the grasp success rate and set the acceptance threshold $\gamma = 0.1$ for all of our other experiments.

VI. CONCLUSION

We present GP-net, a model to propose 6-DOF grasps based on depth images with a mobile manipulator. In contrast to widely used algorithms for robotic grasping like GPD [11] and VGN [8], GP-net does not need a pre-defined workspace or grasp filtering to produce good grasp proposals. Hence, GP-net can be used out-of-the-box on mobile robots without additional steps like plane-fitting, table segmentation or 3D object detection. To train GP-net, we create a synthetic dataset based on 1400 object meshes with ground-truth grasp information.

We evaluate GP-net on a PAL TIAGo mobile manipulator in real-world experiments and compare its performance to GPD and VGN on 9 objects of the EGAD! grasping benchmark [16]. GP-net achieves a grasp success rate of 82.2%, significantly higher than VGN’s 57.8% and GPD’s 63.3% in our setup.

A limitation of GP-net is the gripper-dependence of our dataset and hence the model, similar to most of the commonly used methods [8]–[10]. Since the quality of grasps depends on the grasp being collision-free, the design of the gripper is used implicitly during dataset generation when checking for collisions, see Eq. 2. The resulting model learns the implicit gripper design and hence the performance on alternative gripper configurations cannot be guaranteed. Other setups would likely require the generation of a new dataset and training of a new model.

In future work, we aim to extend GP-net to usage with multiple objects on planar surfaces. More realistic scenarios would include a variety of objects in clutter, for which an extension of GP-net would provide collision-free grasp proposals for the objects that should be retrieved.

REFERENCES

- [1] J. Bohg, A. Morales, T. Asfour, and D. Kragic, "Data-driven grasp synthesis—a survey," *IEEE Transactions on Robotics*, vol. 30, no. 2, pp. 289–309, April 2014.
- [2] J. Mahler, J. Liang, S. Niyaz, M. Laskey, R. Doan, X. Liu, J. A. Ojea, and K. Goldberg, "Dex-net 2.0: Deep learning to plan robust grasps with synthetic point clouds and analytic grasp metrics," in *Robotics: Science and Systems (RSS)*, 2017.
- [3] J. Zhang, M. Li, Y. Feng, and C. Yang, "Robotic grasp detection based on image processing and random forest," *Multimedia Tools and Applications*, vol. 79, 01 2020.
- [4] V. Satish, J. Mahler, and K. Goldberg, "On-policy dataset synthesis for learning robot grasping policies using fully convolutional deep networks," *IEEE Robotics and Automation Letters*, 2019.
- [5] D. Morrison, P. Corke, and J. Leitner, "Learning robust, real-time, reactive robotic grasping," *The International Journal of Robotics Research*, vol. 39, no. 2-3, pp. 183–201, 2019. [Online]. Available: <https://doi.org/10.1177/0278364919859066>
- [6] J. Redmon and A. Angelova, "Real-time grasp detection using convolutional neural networks," in *2015 IEEE International Conference on Robotics and Automation (ICRA)*, 2015, pp. 1316–1322.
- [7] S. Kumra, S. Joshi, and F. Sahin, "Antipodal robotic grasping using generative residual convolutional neural network," in *2020 IEEE/RSJ International Conference on Intelligent Robots and Systems (IROS)*, 2020, pp. 9626–9633.
- [8] M. Breyer, J. J. Chung, L. Ott, S. Roland, and N. Juan, "Volumetric grasping network: Real-time 6 dof grasp detection in clutter," in *Conference on Robot Learning*, 2020.
- [9] M. Sundermeyer, A. Mousavian, R. Triebel, and D. Fox, "Contact-graspnet: Efficient 6-dof grasp generation in cluttered scenes," in *2021 IEEE International Conference on Robotics and Automation (ICRA)*, 2021, pp. 13 438–13 444.
- [10] J. Lundell, F. Verdoja, and V. Kyrki, "Beyond top-grasps through scene completion," in *2020 IEEE International Conference on Robotics and Automation (ICRA)*, 2020, pp. 545–551.
- [11] A. ten Pas, M. Gualtieri, K. Saenko, and R. Platt, "Grasp pose detection in point clouds," *The International Journal of Robotics Research*, vol. 36, no. 13-14, pp. 1455–1473, 2017. [Online]. Available: <https://doi.org/10.1177/0278364917735594>
- [12] L. Berscheid, C. Friedrich, and T. Kröger, "Robot learning of 6 dof grasping using model-based adaptive primitives," in *2021 IEEE International Conference on Robotics and Automation (ICRA)*, 2021, pp. 4474–4480.
- [13] S. Levine, P. Pastor, A. Krizhevsky, J. Ibarz, and D. Quillen, "Learning hand-eye coordination for robotic grasping with deep learning and large-scale data collection," *The International Journal of Robotics Research*, vol. 37, no. 4-5, pp. 421–436, 2018. [Online]. Available: <https://doi.org/10.1177/0278364917710318>
- [14] U. Viereck, A. Pas, K. Saenko, and R. Platt, "Learning a visuomotor controller for real world robotic grasping using simulated depth images," in *Conference on Robot Learning*. PMLR, 2017, pp. 291–300.
- [15] J. Ichnowski*, Y. Avigal*, J. Kerr, and K. Goldberg, "Dex-NeRF: Using a neural radiance field to grasp transparent objects," in *Conference on Robot Learning (CoRL)*, 2020.
- [16] D. Morrison, P. Corke, and J. Leitner, "Egad! an evolved grasping analysis dataset for diversity and reproducibility in robotic manipulation," *IEEE Robotics and Automation Letters*, vol. 5, no. 3, pp. 4368–4375, 2020.
- [17] K. Kleeberger, R. Bormann, W. Kraus, and M. F. Huber, "A survey on learning-based robotic grasping," *Current Robotics Reports*, pp. 1–11, 2020.
- [18] I. Lenz, H. Lee, and A. Saxena, "Deep learning for detecting robotic grasps," *The International Journal of Robotics Research*, vol. 34, no. 4-5, pp. 705–724, 2015. [Online]. Available: <https://doi.org/10.1177/0278364914549607>
- [19] U. Asif, J. Tang, and S. Harrer, "EnsembleNet: Improving grasp detection using an ensemble of convolutional neural networks," in *BMVC*, 2018, p. 10.
- [20] J. Varley, C. DeChant, A. Richardson, J. Ruales, and P. Allen, "Shape completion enabled robotic grasping," in *2017 IEEE/RSJ International Conference on Intelligent Robots and Systems (IROS)*, 2017, pp. 2442–2447.
- [21] Z. Jiang, Y. Zhu, M. Svetlik, K. Fang, and Y. Zhu, "Synergies between affordance and geometry: 6-dof grasp detection via implicit representations," *Robotics: science and systems*, 2021.
- [22] W. Chen, H. Liang, Z. Chen, F. Sun, and J. Zhang, "Transsc: Transformer-based shape completion for grasp evaluation," 2021.
- [23] P. Robotics, "Tiago technical specifications," 2021, last accessed 17 September 2021. [Online]. Available: [https://pal-robotics.com/wp-content/uploads/2021/07/Datasheet-complete-{\\$_\\$}TIAGO-2021.pdf](https://pal-robotics.com/wp-content/uploads/2021/07/Datasheet-complete-{$_$}TIAGO-2021.pdf)
- [24] T. Yamamoto, T. Nishino, H. Kajima, M. Ohta, and K. Ikeda, "Human support robot (hsr)," in *ACM SIGGRAPH 2018 Emerging Technologies*, ser. SIGGRAPH '18. New York, NY, USA: Association for Computing Machinery, 2018. [Online]. Available: <https://doi.org/10.1145/3214907.3233972>
- [25] A. Eitel, J. T. Springenberg, L. Spinello, M. Riedmiller, and W. Burgard, "Multimodal deep learning for robust rgb-d object recognition," in *2015 IEEE/RSJ International Conference on Intelligent Robots and Systems (IROS)*, 2015, pp. 681–687.
- [26] J. Kuffner, "Effective sampling and distance metrics for 3d rigid body path planning," in *IEEE International Conference on Robotics and Automation, 2004. Proceedings. ICRA '04. 2004*, vol. 4, 2004, pp. 3993–3998 Vol.4.
- [27] W. Wohlkinger, A. Aldoma, R. B. Rusu, and M. Vincze, "3dnet: Large-scale object class recognition from cad models," in *2012 IEEE International Conference on Robotics and Automation*, 2012, pp. 5384–5391.
- [28] A. Kasper, Z. Xue, and R. Dillmann, "The kit object models database: An object model database for object recognition, localization and manipulation in service robotics," *The International Journal of Robotics Research*, vol. 31, no. 8, pp. 927–934, 2012. [Online]. Available: <https://doi.org/10.1177/0278364912445831>
- [29] J. Pages, L. Marchionni, and F. Ferro, "Tiago: the modular robot that adapts to different research needs," in *International workshop on robot modularity, IROS*, 2016.
- [30] C. Eppner, A. Mousavian, and D. Fox, "ACRONYM: A large-scale grasp dataset based on simulation," in *2021 IEEE Int. Conf. on Robotics and Automation, ICRA*, 2020.
- [31] D. Seita, F. T. Pokorny, J. Mahler, D. Kragic, M. Franklin, J. Canny, and K. Goldberg, "Large-scale supervised learning of the grasp robustness of surface patch pairs," in *2016 IEEE International Conference on Simulation, Modeling, and Programming for Autonomous Robots (SIMPAN)*, 2016, pp. 216–223.
- [32] J. Mahler, F. T. Pokorny, B. Hou, M. Roderick, M. Laskey, M. Aubry, K. Kohlhoff, T. Kröger, J. Kuffner, and K. Goldberg, "Dex-net 1.0: A cloud-based network of 3d objects for robust grasp planning using a multi-armed bandit model with correlated rewards," in *IEEE International Conference on Robotics and Automation (ICRA)*. IEEE, 2016, pp. 1957–1964.
- [33] J. Weisz and P. K. Allen, "Pose error robust grasping from contact wrench space metrics," in *2012 IEEE International Conference on Robotics and Automation*, 2012, pp. 557–562.
- [34] A. Konrad, J. McDonald, and R. Villing, "Vgq-cnn: Moving beyond fixed cameras and top-grasps for grasp quality prediction," in *to appear in 2022 IEEE International Joint Conference on Neural Networks*, 2022.
- [35] A. Handa, T. Whelan, J. McDonald, and A. J. Davison, "A benchmark for rgb-d visual odometry, 3d reconstruction and slam," *ICRA*, 2014.
- [36] J. T. Barron and J. Malik, "Intrinsic scene properties from a single rgb-d image," *CVPR*, 2013.
- [37] A. Ten Pas and R. Platt, "Using geometry to detect grasp poses in 3d point clouds," in *Robotics Research*. Springer, 2018, pp. 307–324.
- [38] E. Coumans and Y. Bai, "Pybullet, a python module for physics simulation for games, robotics and machine learning," <http://pybullet.org>, 2016–2021.